Supplementary Information

Tailoring the phase transition of silver selenide at the atomics scale

Chen Luo, Zuoyuan Dong, Tao Xu, Xin Yang, Hui Zhang, Hengchang Bi, Chaolun Wang, Litao Sun, Junhao Chu, Xing Wu

Dr. C. Luo, Z. Dong, X. Yang, Prof. H. Bi, Ass. Prof. C. Wang, Prof. J. Chu, Prof. X. Wu

Shanghai Key Laboratory of Multidimensional Information Processing, School of Communication and Electronic Engineering, East China Normal University, Shanghai 200241, China

Dr. C. Luo, Prof. J. Chu

Institute of Optoelectronics, Fudan University, Shanghai 200433, China

Ass. Prof. T. Xu, Dr. H. Zhang, Prof. L. Sun

SEU-FEI Nano-Pico Center, Key Laboratory of MEMS of Ministry of Education, School of Electronic Science and Engineering, Southeast University, Nanjing 210096, China

Keywords: phase transition, silver selenide, in situ, transmission electron microscopy

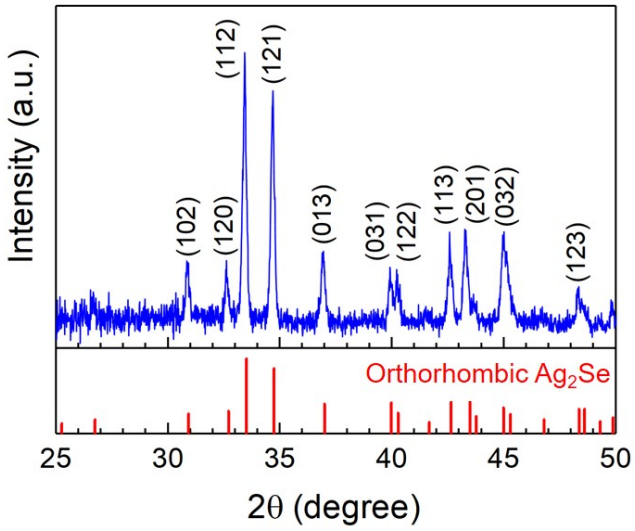

Figure S1. XRD result of the initial orthorhombic Ag_2Se (bulk).

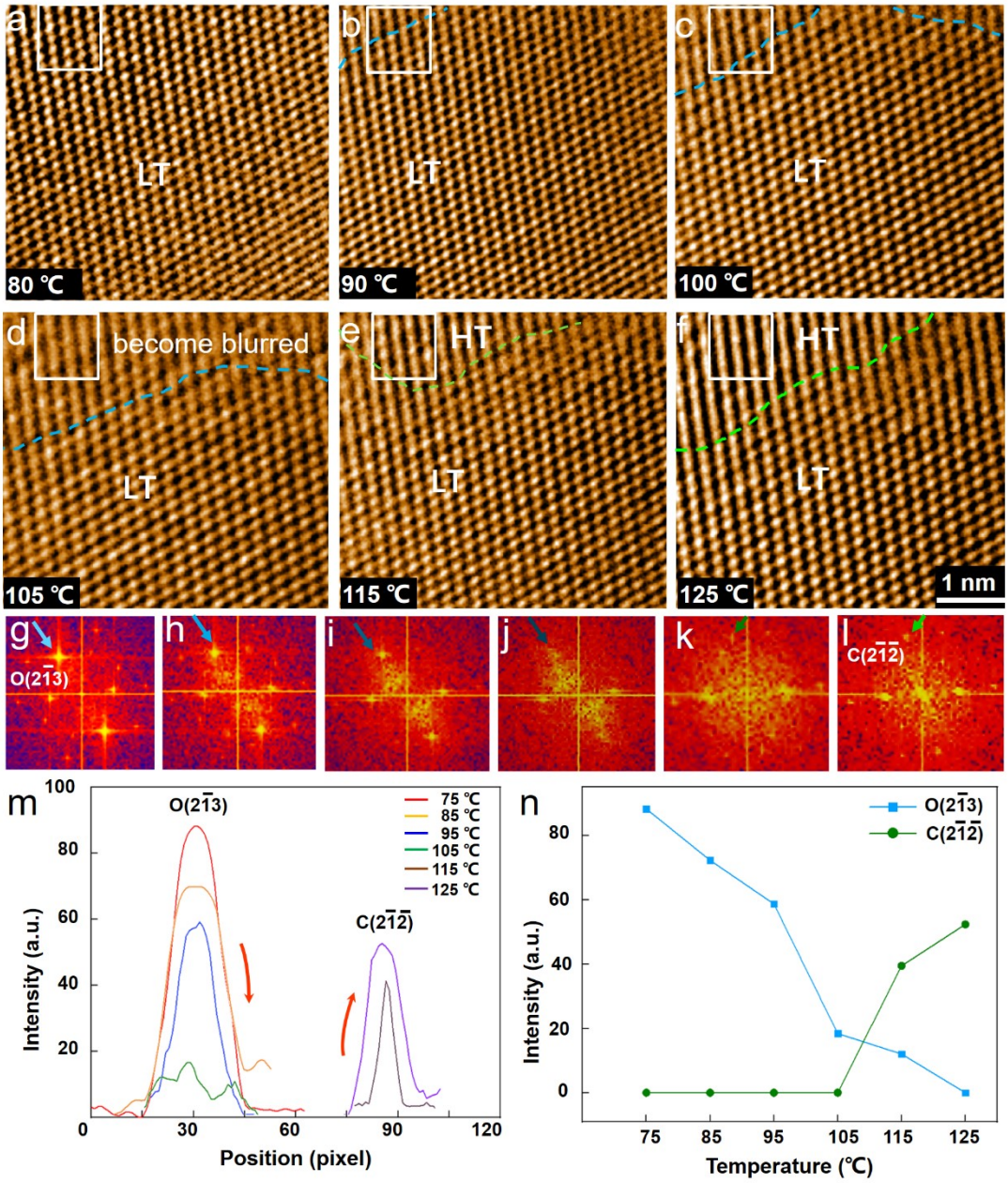

Figure S2. a-d) The local atomic migration process. e-f) The nucleation of the cubic phase. g-l) The corresponding FFT images. m-n) The evolution of the intensity of the diffraction patterns of O(2-13) and C(2-1-2).

Figure S2 exhibits the local atomic migration process and nucleation process of the cubic phase in detail. During the local atomic migration process, the LT diffraction

patterns become blurred and the intensity decreases, as shown in Figure S2g-j. It indicates the decrease of the crystalline order. When the nucleation of the HT phase, the diffraction patterns belonging to the HT phase appear and become sharp, as shown in Figure S2k-l. To demonstrate this process quantitatively, the amount of crystalline order determined from the FFT patterns is used. The quantitative intensity analysis is shown in Figure S2m-n.

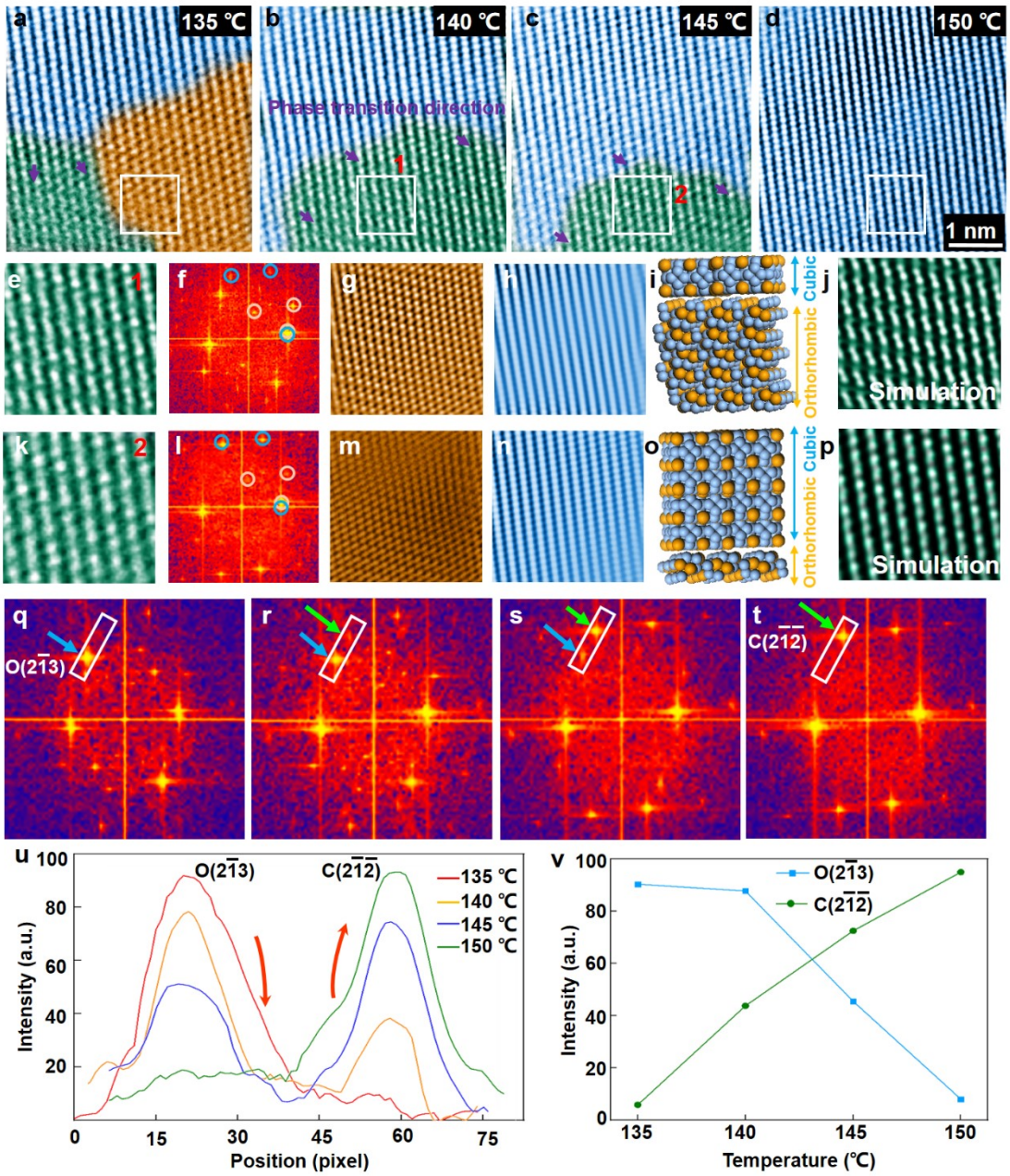

Figure S3. a-d) The growth process of the cubic phase from 135 °C to 150 °C. e-j) The detailed analysis and simulation of position 1 in Figure S3b. k-p) The detailed analysis and simulation of position 2 in Figure S3c. q-t) The corresponding FFT images. u-v) The evolution of the intensity of the diffraction patterns of O(2-13) and C(2-1-2).

Figure S3 exhibit the growth process of the cubic phase. From the FFT result shown in Figure S3f,l, the co-existence phase consists of the LT phase and HT phase. Then, the

position and the intensity of characteristic diffraction patterns are selected to separate and reconstruct the LT and HT phases respectively during phase transition using the inverse fast Fourier transform (IFFT) method, as shown in Figure S3e-p. Through the comparison of the reconstructed LT phase (HT phase) IFFT image at different temperatures, differences in crystalline order can be observed, as shown in Figure S3e-h, k-n. The atoms in Figure S3g,n are clearly and periodically arranged, while the atoms in Figure S3h,m are blurred. It indicates the decrease of LT phase and the increase of HT phase. That is to say, the phase transitions from LT phase to HT phase is not only along the in-plane direction, but also along the out-of-plane direction. To confirm the result, two vertical stacking models with different proportion of LT phase and HT phase is constructed, as shown in Figure S3i,o. Based on two models, the corresponding HRTEM images are simulated, as shown in Figure S3j,p. The simulated HRTEM results match well with the experimental results. Figure S3q-t show the FFT analysis of the vertical phase transition process, and the quantitative intensity analysis is shown in Figure S3u-v.

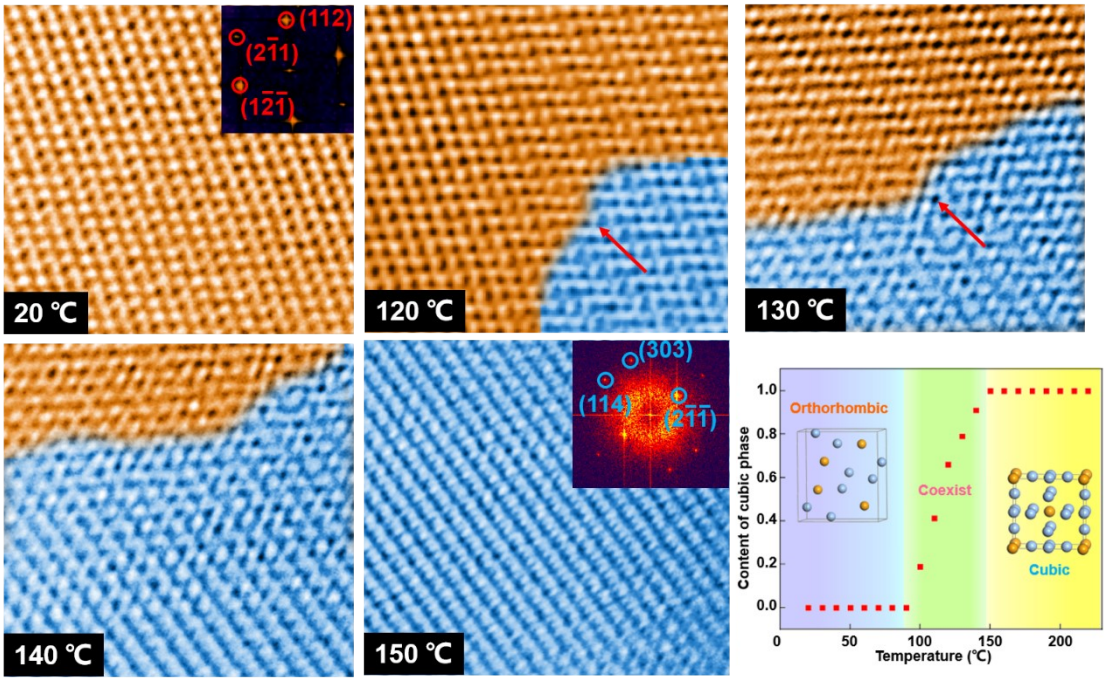

Figure S4. Another case of the phase transition from LT phase to HT phase at the increased temperature.

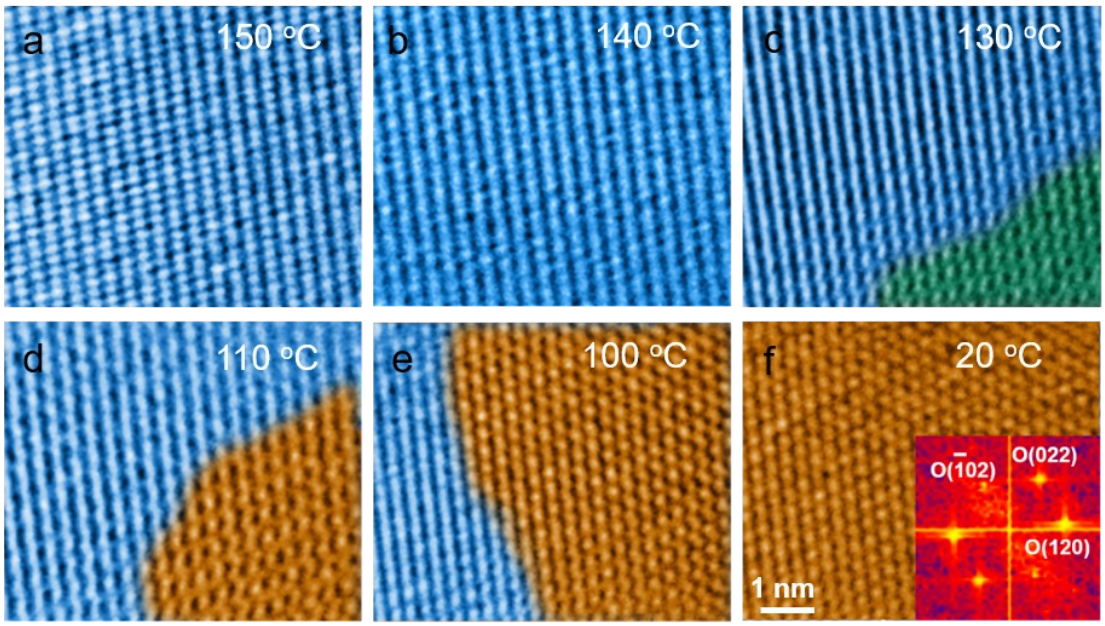

Figure S5. The phase transition from HT phase to LT phase when the temperature decreases to room temperature.

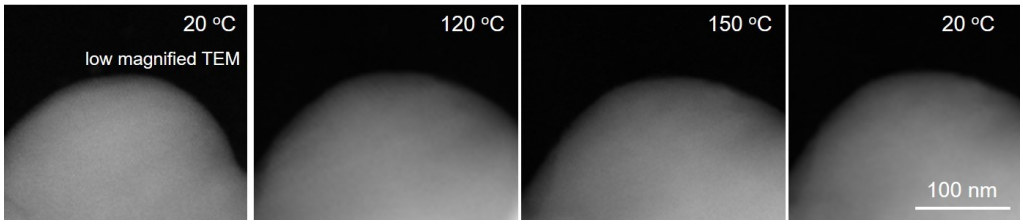

Figure S6 In situ low magnified TEM image of the reversible phase transition process.

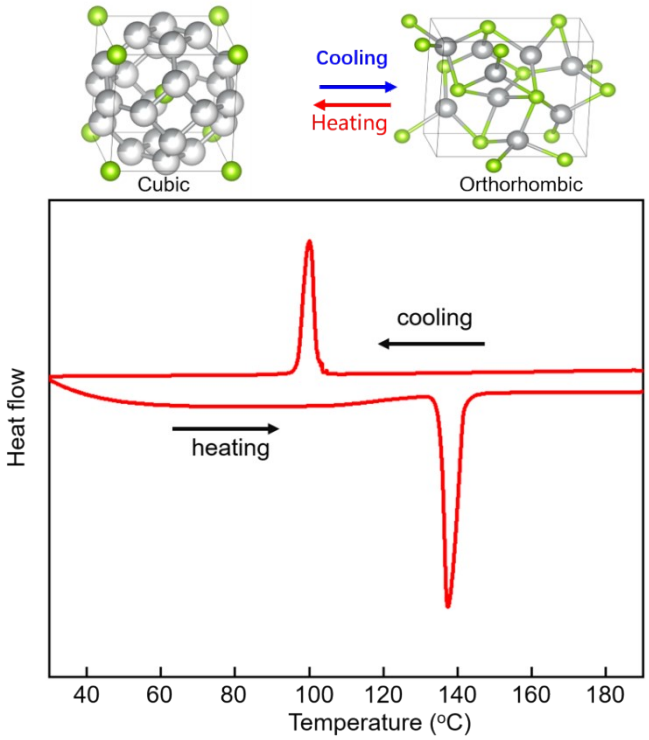

Figure S7. Differential scanning calorimeter (DSC) thermogram.

In general, thermal hysteresis exists in a first-order phase transition in the temperature change experiment, because different solid phases (with different activation barriers) are nucleating and growing during heating and cooling. According to the thermodynamic formula,

$$\Delta G=\Delta H-T\Delta S$$

where G is Gibbs free energy, H is enthalpy, S is entropy, and T is temperature. When the two phases are in equilibrium,

$$\Delta G=\Delta H-T_m\Delta S=0$$

Hence,

$$\Delta S=\Delta H/T_m$$

where T_m is the equilibrium temperature.

When the system is not in equilibrium, then

$$\Delta G=\Delta H-T\Delta S\neq 0$$

That is

$$\Delta G=\Delta H-T(\Delta H/T_m)=\Delta H\cdot(T_m-T)/T_m=\Delta H\cdot\Delta T/T_m\neq 0$$

For an endothermic process ($\Delta H>0$), if the phase transition can occur spontaneously ($\Delta G<0$), then $\Delta T<0$, $T>T_m$, which needs overheating. On the contrary, during the exothermic process, $\Delta T>0$, which needs undercooling. This explains why the phase transition temperature is higher during heating and lower during cooling.

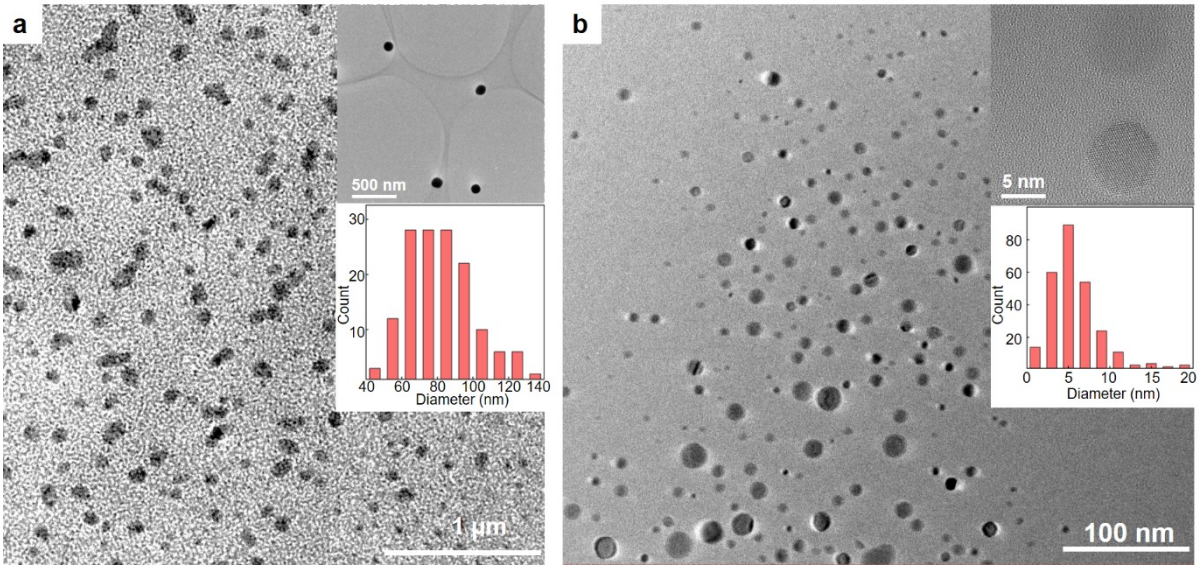

Figure S8. a) The morphology of the Ag_2Se nanoparticles. The diameter of nanoparticles is between 40-139 nm. b) The diameter of nanoparticles is between 2-20 nm.

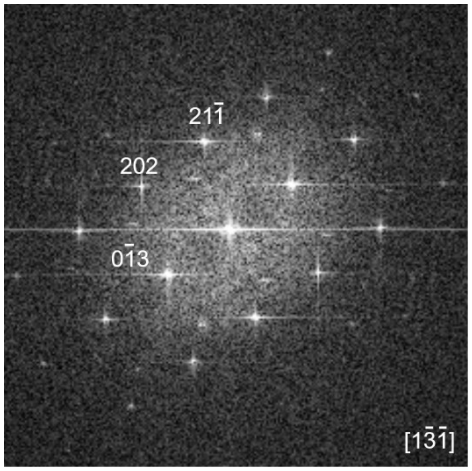

Figure S9. The FFT image of the nanoparticle in Fig. 3a

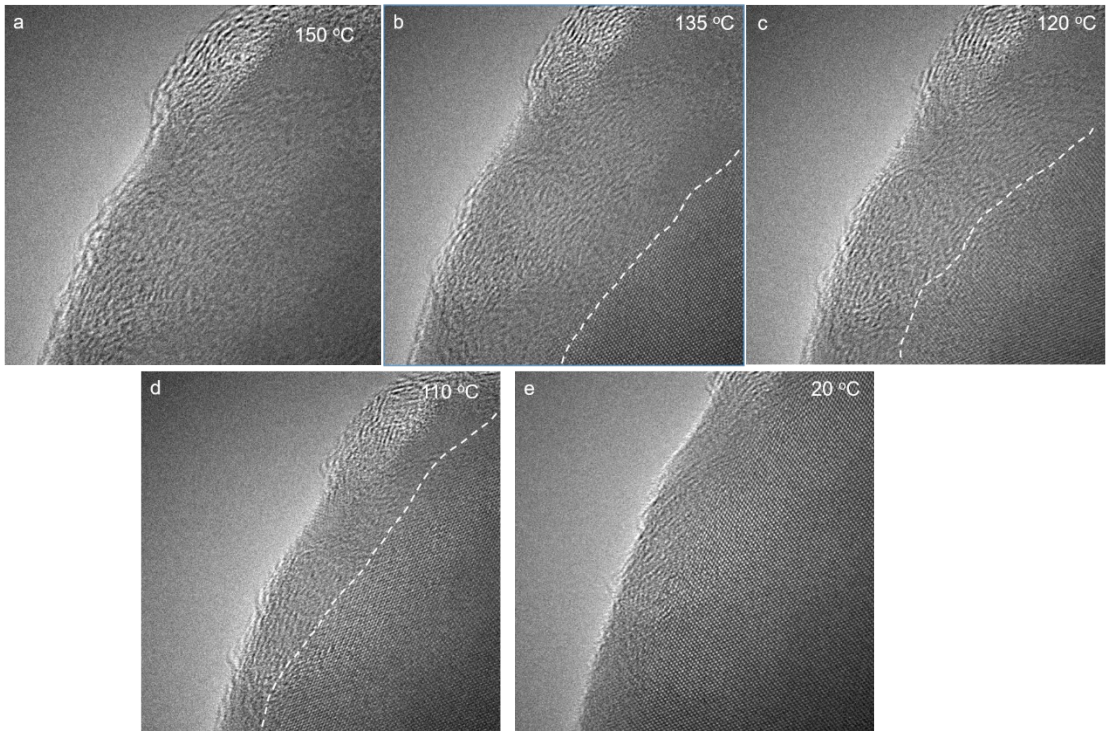

Figure S10. The phase transition from HT phase to LT phase when the temperature decreases to room temperature.

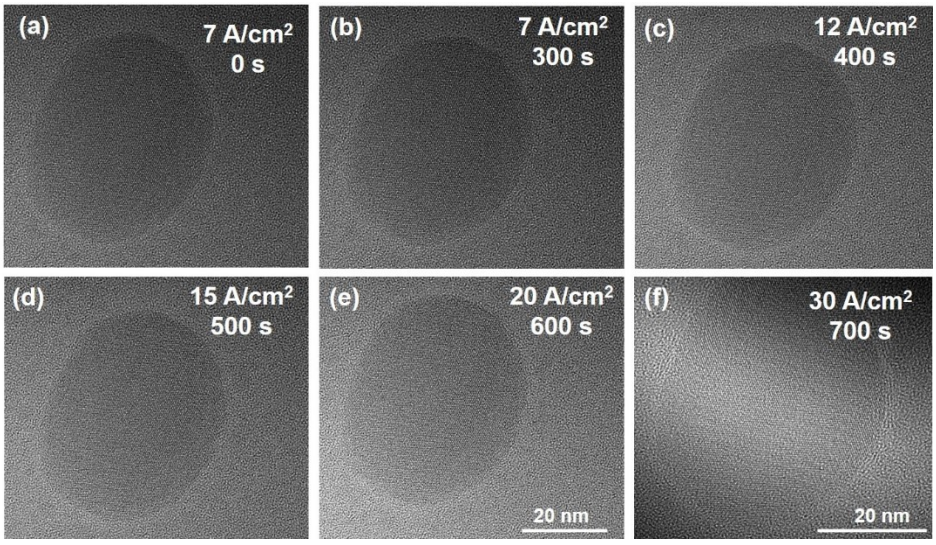

Figure S11. In situ electron beam irradiation experiment, electron beam irradiation effect on phase transition can be ignored.